Communication

Inkjet-printed silicon as high performance anodes for Li-ion batteries

Stephen Lawes[1], Qian Sun[1], Andrew Lushington, Biwei Xiao, Yulong Liu, Xueliang Sun[*]

Department of Mechanical and Materials Engineering, University of Western Ontario, London, Canada N6A 3K7

ABSTRACT

Herein we report the fabrication, optimization, and characterization of inkjet-printed thin film silicon anodes for lithium-ion batteries using commercial silicon nanoparticles. By comparing four different polymer binders, we demonstrate the critical role of binder on achieving good electrochemical performance of inkjet-printed silicon electrodes. Inkjet-printed silicon nanoparticle electrodes with conductive polymer PEDOT:PSS binder exhibit superior performance and durablity, with a capacity retention of over 1000 cycles at a depth-of-discharge of 1000 mA h g^{-1}. The working mechanism of the impact of the binders on inkjet-printed silicon electrodes is investigated and explained in detail via various characterization techniques, including scanning electron microscopy, Raman and infrared spectroscopy.

1. Introduction

Portable energy storage has been receiving worldwide interest as the recent demand for mobile power sources has sky-rocketed. With the miniaturization of wireless devices, rechargeable batteries have had to decrease in size without compromising the amount of energy stored. Thin film batteries are poised to meet this challenge, as they exhibit a number of unparalleled features including high energy and power densities [1,2], short ion diffusion lengths [3,4], and intrinsic flexibility [5,6]. The successful development of high capacity thin film batteries will enable advances in the fields of wireless sensors, RFID tags, implantable medical devices, and robotics. Up to now thin film batteries have mostly been fabricated by traditional thin film growth technologies such as physical vapour deposition (PVD) or chemical vapour deposition (CVD). However, these methods generally require expensive equipment and harsh conditions for thin film growth, including high vacuum or high temperatures, which limits the wide adoption of thin film batteries.

Inkjet printing is a promising technique for fabricating thin film electrodes. It can be used to deposit films of precisely controlled thickness, which can be tuned by the number of layers printed on top of one another. It has many advantages over other thin film fabrication techniques, including ease of use, cost-effectiveness, minimal wasted material, scalability, and the ability to deposit patterns easily. It does not require expensive equipment and deposition can be performed at room temperature and ambient conditions. For these reasons, inkjet printing has been successfully developed to fabricate supercapacitors [7–9], transistors [10,11], solar cells [12–14], and battery electrodes

[15–19]. However, current research on inkjet-printed fabrication of thin film electrodes for lithium-ion batteries (LIBs) has mainly focused on the cathode, while few studies have focused on the anode (Table S1). Zhao et al. reported both inkjet-printed SnO_2 and Li_4TiO_{12} thin films as anodes for LIBs [20,21]. Nonetheless, the discharge capacity of these reported thin film anodes (below 1000 mA h g^{-1}) are still insufficient to meet increasing requirements of energy density for future thin film LIBs.

Silicon has been proposed and widely studied as a candidate anode material for LIBs to at least partially replace the state-of-the-art commercial graphite anodes [22–25], due to its high theoretical gravimetric capacity (4200 mA h g^{-1}, compared to 372 mA h g^{-1} for graphite), low lithium insertion/extraction potential, and low cost [26,27]. Accordingly, thin film Si electrodes have also attracted wide research interest for thin film LIBs (Table S2). However, one well-known challenge of Si anode material is its 400% volume expansion upon full lithium insertion [28], causing pulverisation of the particles and loss of electrical contact which results in decreased capacity during cycling. Nano-scale Si is more resistant to mechanical fracture than micro-scale Si [29,30], and many studies have focused on developing novel nanostructured Si electrodes, such as nanowires [31], nanotubes [32], hollow nanospheres [33], and core-shell structures [34,35], to overcome the poor cycling stability of Si. However, the synthesis of these nanostructured Si electrodes typically requires large amounts of energy and is not easily translated to commercial mass production. One simpler alternative strategy is to use a polymer binder that can accommodate the volume expansion of Si nanoparticles (SiNPs) and maintain electron conduction across the electrode. Previous reports
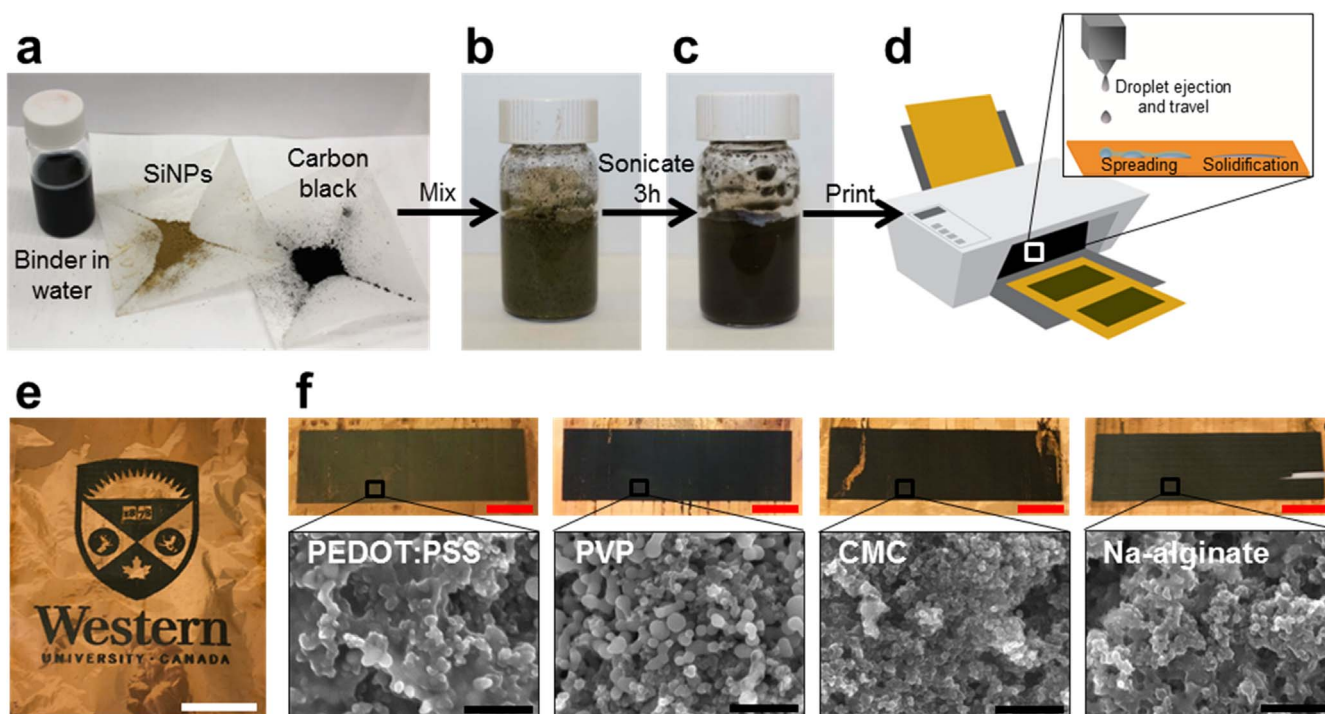
Fig. 1. Procedure used to print SiNP anodes on copper foil. (a, b) First, the ink was prepared by mixing SiNPs, carbon black, and the polymer binder in water. (c) After 3 h of sonication, the solution was well-mixed and (d) injected into an inkjet printer cartridge and printed. (e) Photograph of the Western University logo printed with the SiNP ink. (f) Optical photographs and SEM images of the inkjet-printed SiNP anode films on copper foil. Scale bars red, white, and black represent 3 cm, 5 cm, and 500 nm, respectively.

have shown that the mechanical, chemical, and electronic properties of different binders have a significant effect on the cycling performance of SiNP electrodes [36–41].

Herein we report preparing inkjet-printed SiNP anodes with four commercially available polymer binders, i.e. poly(3,4-ethylenedioxythiophene)-poly(styrene sulfonate) (PEDOT:PSS), polyvinylpyrrolidone (PVP), carboxymethyl cellulose (CMC), and Na-alginate, and investigated their effects on the electrochemical performance of the electrodes in LIBs. We demonstrate that SiNP anodes printed with PEDOT:PSS binder exhibit the most stable cycling at high discharge capacity, due to its excellent jetting properties [42] and electrical conductivity. Scanning electron microscopy (SEM) shows that PEDOT:PSS conformally coats the SiNPs as a conductive layer, allowing for rapid electron transport while binding the electrode together. In addition to the improved electronic conductivity due to the conductive nature of PEDOT:PSS, which has been previously demonstrated as an effective binder for battery electrodes [43–47], we also noticed the unexpected behaviour of PEDOT:PSS acting as a self-healing polymer. Using various characterization techniques, including SEM, Fourier transform infrared (FTIR) spectroscopy, and Raman spectroscopy, we observed the PEDOT:PSS binder stretching during cell discharge to effectively accommodate the volume expansion of SiNPs and shrinking during charge to preserve the continuous conductive network. Thereby, the optimized inkjet-printed SiNP electrode exhibits high electrochemical performance as an anode for Li-ion batteries.

2. Experimental

2.1. Silicon ink preparation

Inks were prepared by mixing SiNPs (50 nm, Hongwu Nano), carbon black (50 nm, Gunbai), and polymer binder at a ratio of 2:2:1 by weight in an appropriate volume of DI-water to achieve a viscosity of 10 mPa s, as measured with a U-tube viscometer (Cannon Instrument Company). Four polymer binders were used: PEDOT:PSS (Sigma-

Aldrich), PVP (Sigma-Aldrich), CMC (Calbiochem), and sodium alginate (Sigma-Aldrich). Inks were sonicated for at least 3 h to break up large agglomerates and ensure uniform dispersion prior to use.

2.2. Electrode and coin cell preparation

The ink was transferred into a well-cleaned HP 61 ink cartridge and printed using a Hewlett-Packard Deskjet 2540 inkjet printer. Twenty-five layers of each ink were printed on copper foil to ensure sufficient thickness and uniformity. After printing, the films were dried in a vacuum oven at 60 °C overnight. The printed films were then cut and assembled in CR-2032 coin cells with lithium metal foil as the counter electrode in an argon-filled glove box. The mass loading of Si in the inkjet-printed thin film electrodes are around 125 μg cm^{-2}. The two electrolytes used were composed of 1 M LiPF$_6$ salt dissolved in different solvent mixtures: (1) 1:1:1 ratio by volume ethylene carbonate, diethyl carbonate, and ethyl methyl carbonate (EC:DEC:EMC) and (2) 1:9 ratio by weight dimethyl carbonate and fluoroethylene carbonate (FEC:DMC). The coin cells were stored overnight at room temperature before testing.

2.3. Characterization

A field emission SEM (Hitachi S-4800) equipped with an energy dispersive X-ray (EDX) spectrometer was used to observe the microstructure and elemental composition of the printed films. Galvanostatic charge-discharge measurements were performed on an Arbin BT-2000 Battery Tester between 0.01 and 1.0 V vs. Li/Li$^+$. The charge/discharge rates and capacities were calculated based on the mass of Si in the anode, as determined by thermogravimetric analysis (TGA, TA Instruments SDT Q600) (see Fig. S1). Cyclic voltammetry (CV) (Fig. S2) and EIS were performed on a multichannel potentiostat 3/Z (VMP3). FTIR spectroscopy (Nicolet 6700) and Raman spectroscopy (532.4 nm laser, HORIBA Scientific LabRAM HR) were performed to analyze anodes with PEDOT:PSS binder before cycling, after first cycle lithiation, and after first cycle delithiation.

3. Results and discussion

3.1. Electrode fabrication

Inkjet printing is a simple method to produce highly uniform thin film electrodes with tunable thicknesses. All inks were prepared with commercially available materials without modification. Ink formulations were comprised of three materials: an electrochemically active material, SiNPs; a conducting agent, carbon black; and one of four polymer binders (Fig. 1**a**). These components were mixed in water (Fig. 1**b**) and then sonicated for several hours during which large agglomerations of particles were broken up, resulting in a dark brown homogenous suspension (Fig. 1**c**). Inks were then transferred into a well-cleaned ink cartridge and printed onto a copper foil current collector with a commercial desktop inkjet printer (Fig. 1**d**). The inkjet printing process can be divided into three main stages: droplet ejection and travel, droplet spreading, and droplet solidification. The print head is positioned at the desired location and droplets of ink are forced through the nozzles and are deposited onto the substrate. Upon impact, the deposited droplets spread along the surface and join with other droplets to form a thin film of liquid ink. Finally, the solvent evaporates and the solid contents of the ink remain on the substrate. To demonstrate the patternability of the inkjet printing technique, the logo of *Western University* was printed using this SiNP ink on copper foil (Fig. 1**e**). In addition, this printing technique uses aqueous solutions, making it a versatile and safe fabrication method.

Multiple printing passes were performed to achieve highly uniform films of desired thickness. Printing too few passes resulted in non-uniform films with isolated islands of deposited material, while printing too many passes reduced the electrode's capacity due to higher internal cell resistance (Fig. S3), consistent with previous reports [48]. The optical images in Fig. 1**f** show printed films with 25 layers using the four different polymer binders, along with SEM images demonstrating their morphological differences. These four films were all around 1 μm thick, as measured by cross-sectional SEM. The thickness and tap density of the electrodes are important parameters for achieving high volumetric energy density in thin film batteries, and may be further improved by mechanical pressing [49]. The thicknesses and loadings of the inkjet-printed SiNP thin film electrodes reported here are comparable with both the previously reported other electrode materials fabricated by inkjet-printing (Table S1) and Si-based thin film electrodes fabricated by other methods (Table S2). It can be observed that the printed SiNP anodes with PEDOT:PSS binder are built of a continuous polymer network, with SiNPs embedded in the matrix. In contrast, the inkjet-printed SiNP anodes with PVP, CMC, and Na-alignate binders created more discontinuous films containing isolated particles. Moreover, EDX spectroscopy mapping demonstrates the uniform distribution of SiNPs within each film (Fig. S4).

### 3.2. Electrochemical performance

To characterize the electrochemical properties of the inkjet-printed silicon anodes with different polymer binders, deep galvanostatic cycling measurements were performed on printed SiNP/metallic Li half cells between 0.01 and 1 V at a current rate of 0.1 C (where 1 C=4200 mA g^{-1}). The results are shown in Fig. 2. It can be observed that SiNP anodes with PEDOT:PSS binder exhibited both large initial and reversible capacity, as well as the most stable cycling performance (Fig. 2**a**), comparable to the best reported electrochemical performance of thin film SiNP electrodes fabricated via other methods (Table S2). Although the SiNP anodes with PVP binder also exhibited large first-cycle discharge capacities similar to anodes with PEDOT:PSS binder, the subsequent discharge capacity rapidly decayed within ten cycles. In contrast, the SiNP anodes with CMC and sodium alginate binders both displayed low initial capacities that quickly dropped to nearly zero within two or three cycles. These observations are consistent with the

CV curves shown in Fig. S2, which show better reversibility for the SiNP anode with PEDOT:PSS binder, compared to Si anodes with the other binders. In addition, the reduction and oxidation currents in the CV curves are higher for the anode with PEDOT:PSS, indicating a greater amount of reversible active silicon present in the electrode. This may be due to low electron conduction through the electrode with the insulating binders (PVP, CMC, and Na-alginate), resulting in electrical isolation of SiNPs not adjacent to the current collector, possibly as a result of poor ink-jetting compatibility of these polymer binders. All of the inkjet-printed SiNP anodes with the four different binders demonstrated an irreversible capacity loss during the first cycle, which can be attributed to solid electrolyte interphase (SEI) formation. PEDOT:PSS contributed to part of the initial irreversible capacity loss but added little capacity in subsequent cycles, as shown by the cycling performance of a PEDOT:PSS-only electrode in Fig. S5. Except for this initial capacity loss, inkjet-printed SiNP anodes with PEDOT:PSS show very stable performance for 100 cycles.

To highlight the excellent cycling performance of the inkjet-printed silicon anodes with PEDOT:PSS binder and to provide a comparison of these anodes in two common commercial electrolyte systems for LIBs, cells were tested with both EC:DEC:EMC and DMC:FEC electrolyte systems. The EC:DEC:EMC electrolyte is common for traditional LIBs with graphite anodes, while DMC:FEC electrolyte gives improved performance for LIBs with silicon anodes. The stabilizing effect of FEC has been previously reported and is attributed to the formation of a more stable SEI layer that prevents cracking during volume changes [50,51]. The cells with electrolyte containing DMC:FEC demonstrated increased stability compared to those with electrolyte containing EC:DEC:EMC, with 100th cycle capacities of 1714 mA h g^{-1} and 961 mA h g^{-1} based on the mass of silicon, respectively. The thin film SiNP anodes with PEDOT:PSS binder and DMC:FEC electrolyte were also cycled at 1 C and show good electrochemical performance for 100 cycles (Fig. S6).

The voltage profiles of printed anodes using PEDOT:PSS binder and DMC:FEC electrolyte are shown in Fig. 2**b**. The first cycle exhibits a long plateau around 0.1 V during lithiation, characteristic of crystalline silicon. Subsequent cycles have sloping plateau regions between 0.3 and 0.01 V *vs.* Li/Li$^+$, indicative of lithium insertion into amorphous Li$_x$Si [52]. Moreover, the specific capacity of an inkjet-printed silicon anode with PEDOT:PSS binder varied from 2500 mA h g^{-1} at 0.1 C to 900 mA h g^{-1} at 5 C (Fig. 2**c**). Even at a charge/discharge rate of 2 C, a sloping plateau region is observed between 0.25 and 0.01 V *vs.* Li/Li$^+$(Fig. 2**d**), similar to those shown in Fig. 2**b**. This demonstrates the ability of lithium ions to rapidly penetrate the PEDOT:PSS coating and alloy with the silicon at high cycling rates. The reason may be attributed to the fact that PEDOT:PSS forms a continuous conductive network that connects SiNPs to the current collector, providing rapid electron transport at elevated current densities. No obvious plateau is observed in the charging profile when cycling at 5 C, due to further increased polarization under high current densities.

Capacity limited depth-of-discharge measurements were also carried out to a capacity cut-off of 1000 mA h g^{-1} at 0.1 C (Fig. 2**e**) between 0.01 and 2.5 V. The inkjet printed SiNP with PEDOT:PSS binder/Li cell lasted 150 cycles at the cut-off capacity of 1000 mA h g^{-1} before fading in EC:DEC:EMC electrolyte. When using DMC:FEC electrolyte, printed SiNP anodes with PEDOT:PSS binder exhibited further prolonged cycling stability, with over 1000 cycles at the cut-off capacity of 1000 mA h g^{-1} (Fig. 2**e**). This can be attributed to formation of less stable SEI in the EC-based electrolyte than those formed in the FEC-based electrolyte. To compare the inkjet-printed SiNP electrode to conventional Si electrodes for Li-ion batteries, SiNP anodes with Na-alginate and poly(vinylidene fluoride) (PVDF) binders were also prepared using the conventional doctor-blade casting method and compared in Fig. 2**e**. These doctor-blade casted SiNP anodes with Na-alginate and PVDF binders failed to maintain a discharge capacity of 1000 mA h g^{-1} after 22 and 5 cycles, respectively. Previous studies
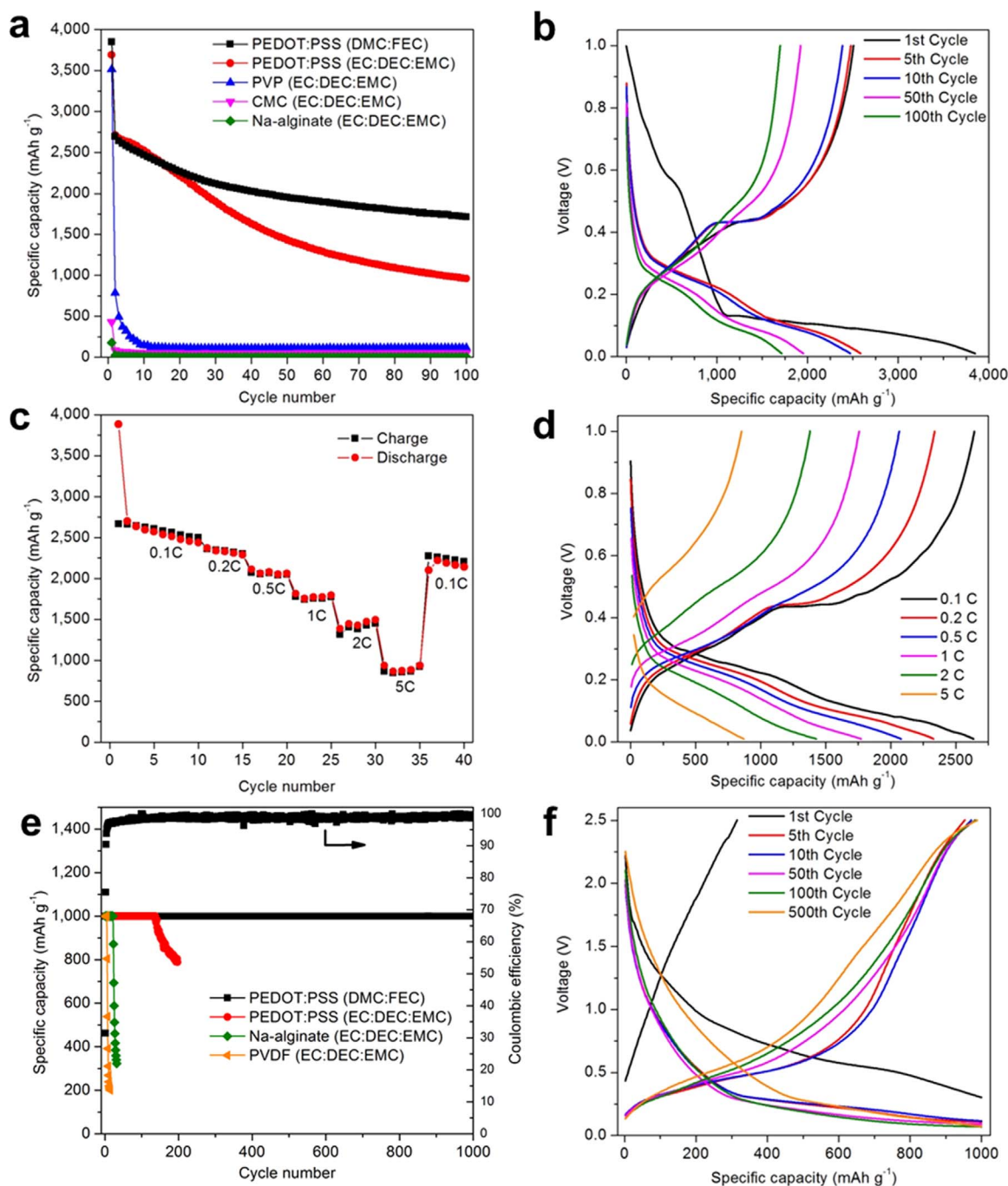
Fig. 2. (a) Cycling performance at 0.1 C of inkjet-printed silicon anodes prepared with four different polymer binders. (b) Voltage profiles of selected cycles for the PEDOT:PSS (DMC:FEC) cell from (a). (c, d) Rate capability measurements of Si anodes with PEDOT:PSS binder in DMC:FEC electrolyte. (e) Limited depth-of-discharge tests performed to a capacity cut-off of 1000 mA h g^{-1}. Si electrodes with PEDOT:PSS binder are fabricated via inkjet printing. The Si electrodes with Na-alginate and PVDF binders were prepared by traditional doctor-blading method to compare. The Coulombic efficiency shown is for the Si anode with PEDOT:PSS binder in DMC:FEC electrolyte. (f) Voltage profiles from typical cycles of the Si anode with PEDOT:PSS binder in DMC:FEC electrolyte as shown in (e).

have shown that PVDF is unable to accommodate the large volume changes during the lithiation of silicon, causing the binder to detach from the current collector and leading to increased cell resistance and poor cycling performance [53]. In this study, the doctor-blade casted SiNP electrodes with Na-alginate binder also show improved electro-chemical performance compared to those with PVDF binders made by the same method, which is consistent with previous reports. Nevertheless, they still cannot compete with the SiNP electrodes with PEDOT:PSS binder fabricated by inkjet-printing. Additional cycling tests shown in Fig. S7 were performed to compare the two fabrication methods, namely inkjet printing and doctor-blade casting, using the

same binder, PEDOT:PSS. The inkjet-printed SiNP anodes exhibited higher discharge capacity and better cycling stability than the doctor-bladed SiNP anodes. This comparison indicates the advantage of the application of inkjet printing technology in the field of thin film LIBs.

The Coulombic efficiency (CE) of the SiNP anode with PEDOT:PSS binder in DMC:FEC is 31% and 75% for the first two cycles and increases to around 98.6% for the remaining cycles. Fig. 2**f** shows the voltage profiles of this cell, in which a low first-cycle charge capacity with no plateau is observed. This is due to the irreversible SEI formation that occurs during the first discharge. Normally, SEI formation contributes only a small fraction to the total capacity of

the first discharge. However, for this cell the capacity was cut off at 1000 mAh/g, meaning a larger proportion of its capacity was due to SEI formation, consistent with the large initial capacity loss of the PEDOT:PSS-only anode shown in Fig. S5. Therefore, a lower proportion of the first-cycle discharge capacity was due to the reversible lithiation of silicon, leading to low capacity and no observed plateau on the first charge. The low CE for the first two cycles can be attributed to this irreversible capacity loss from SEI formation. High initial resistance of the cell, as measured by electrochemical impedance spectroscopy (EIS) (Fig. S8), may also contribute to the low first-cycle CE. Once a stable SEI has been formed on the surface of the SiNP electrode, the CE remains constant and the cell continues to exhibit a stable capacity of 1000 mA h g^{-1}. The discharge plateaus (i.e. lithiation of Si) remain relatively constant over the first 100 cycles and all discharge plateaus occur at lower voltages than the first cycle, indicating a lower internal resistance. However, as cycling continues to 500 cycles and beyond, the growth of thicker SEI and the gradual loss of electrical contact between SiNPs and conducting carbon black and PEDOT:PSS leads to increasing polarization and a rise in the voltage plateau.

3.3. Physical characterization

SEM, Raman, and IR characterization was performed at three stages of the charge/discharge cycle of anodes prepared with PEDOT:PSS binder: before cycling, after the 1st lithiation, and after the 1st delithiation. As seen in the SEM images shown in Fig. 3a, the morphology of the pristine anode was a continuous polymer network with embedded SiNPs. Upon lithiation the SiNPs expanded, causing the polymer binder to stretch into a fibrous structure. Very interestingly, after delithiation, the SiNPs together with binder contracted and the morphology of the electrode restored to its pristine condition, indicating that the PEDOT:PSS network remains intact during volume expansion and is able to maintain intimate contact with the SiNPs. The continuous conductive PEDOT:PSS network is preserved, ensuring that all SiNPs remain electrically connected to the current collector, which is critical to the overall electrochemical performance of the electrode. For comparison, SEM images of SiNP anodes with PVP binder are shown in Fig. S9, which do not show the same self-healing behaviour as the PEDOT:PSS binder. This comparison may explain the poor electrochemical performance of inkjet-printed SiNP anodes with PVP binder, which faded rapidly in the initial ten cycles.

Furthermore, this self-healing effect of PEDOT:PSS binder is also consistent with results obtained from FTIR (Fig. 3b) and Raman (Fig. S10) spectroscopy. The IR peaks at 1635 and 667 cm^{-1} represent C=C stretching and C-S stretching in the thiophene ring, respectively [54–56]. Upon lithiation the intensity of both these peaks decreases, indicating reduced stretching vibrations in the thiophene ring of the PEDOT chain. This can be explained by considering the structure of PEDOT:PSS (Fig. 3c). In the initial state, positively-charged thiophene groups exist in the PEDOT molecules and negatively-charged sulfonyl
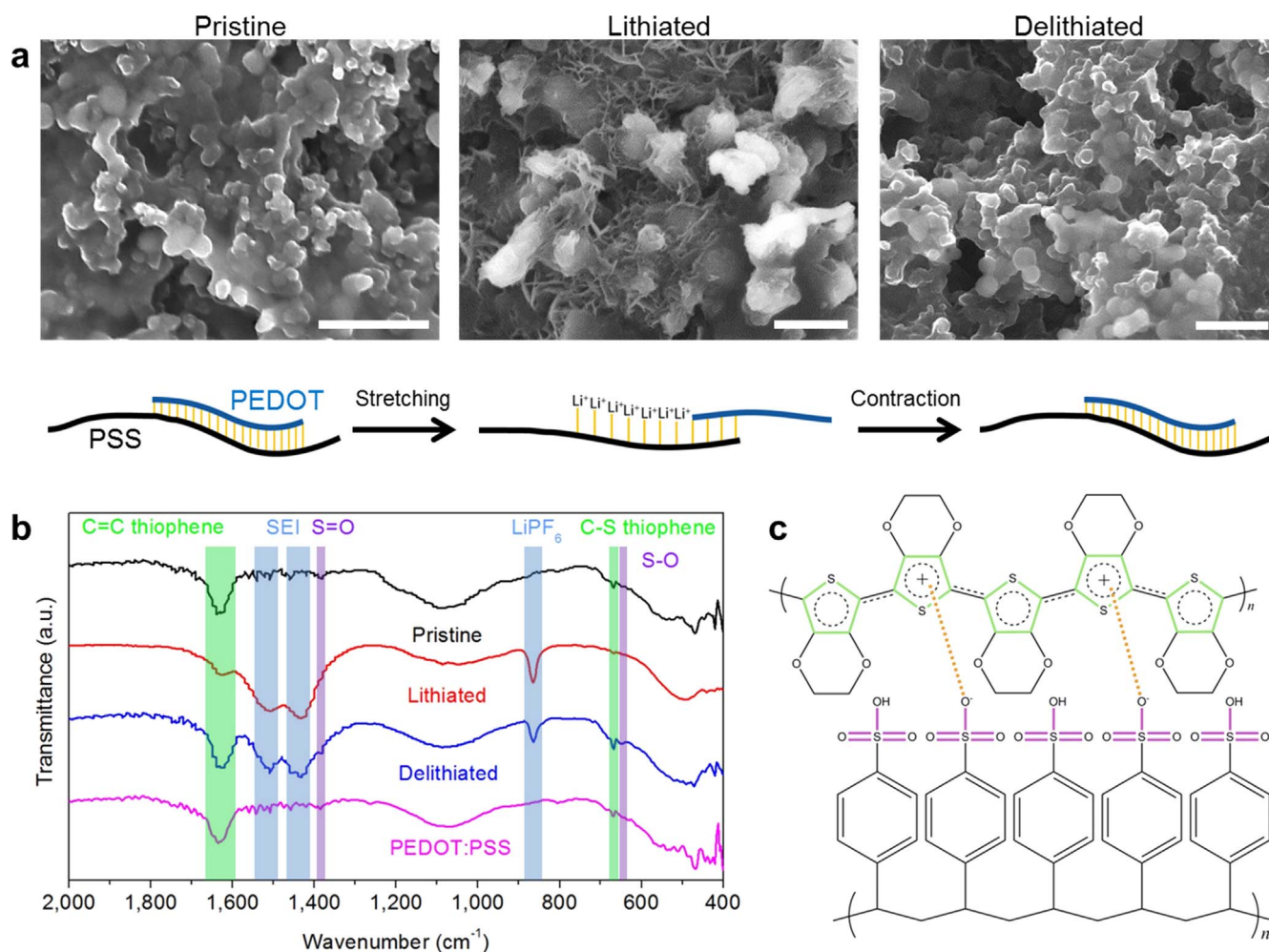
Fig. 3. (a) SEM images and (b) FTIR spectra of SiNP anodes with PEDOT:PSS binder taken at three stages of a discharge/charge cycle: before cycling (pristine), after first discharge (lithiated), and after first full discharge and charge (delithiated). The scale bars in SEM pictures stand for 500 nm. The green highlighted regions in the FTIR spectra indicate the PEDOT:PSS thiophene C=C and C-S stretching vibrations, the blue highlighted regions indicate SEI formation and residual electrolyte salt, and the purple highlighted regions indicate the sulfonic acid groups. (c) The schematic structure of PEDOT:PSS.

groups exist in the PSS molecules, which stabilize one another by electrostatic attraction. The lower electron densities in the positive thiophene rings result in more asymmetric stretching vibrations compared to the neutral thiophene rings. When the polymer chains stretch during lithiation, the PEDOT(+) and PSS(−) chains slide past one another, reducing the interaction between the two polymer units. The decreased number of sulfonyl groups nearby to stabilize positively-charged thiophene rings leads to a decreased number of positive thiophene rings. The increased electron density of the neutral thiophene groups suppresses the asymmetric stretching modes of the C=C and C-S bonds in PEDOT, resulting in a lower IR absorbance. During delithiation, the polymer chains contract, increasing the interaction between PEDOT and PSS molecules and therefore increasing the number of positively-charged thiophene rings, as evident from the return of the IR intensity to that of the pristine state. This explanation is further supported by changes to the IR peaks at 1382 and 648 cm^{-1}, which represent S=O stretching and S-O stretching, respectively [56,57]. Similarly, these peaks are present in the IR spectra of the pristine and delithiated samples, but absent in that of the lithiated electrode. This is due to the suppressed asymmetric stretching of the sulfonic acid groups in PSS when Li^+ ions are available to ionically stabilize the negative sulfonyl groups that were previously paired with the positive thiophene ring in the pristine and delithiated electrodes. These IR results provide more evidence for the mechanism of the self-healing effect of the PEDOT:PSS binder as shown in the SEM images.

The additional peak in the IR spectra at 864 cm^{-1} corresponds to residual $LiPF_6$ [58,59], while the peaks at 1435 and 1508 cm^{-1} are attributable to the formation of Li_2CO_3 or other organic carbonates in the SEI [59,60]. As expected, these peaks appear after lithiation and are not present in the pristine state. The SEI peaks are still present after delithiation, indicating irreversible SEI formation. This also supports the cycling performance results above, in which there is significant irreversible capacity loss after the first cycle. The SEI formed at the PEDOT:PSS binder-electrolyte interface may differ chemically and mechanically from the SEI formed at the Si-electrolyte interface, and it has been suggested that this difference may also contribute to improved cycling stability [61].

4. Discussion

An explanation of the varying electrochemical performance of printed SiNP anodes prepared with different binders is proposed in Fig. 4. There are three different electrode structures that form during the inkjet-printing process, dependent on the binder used:

(1) In the case of CMC and Na-alginate binders, clusters of SiNPs and carbon black are surrounded by the polymer binder, electrically isolating them from each other. There are no electron conduction pathways to these isolated particles, and therefore only SiNPs in direct contact with the current collector are electrochemically active and contribute to energy storage. This results in the low initial capacity of electrodes prepared with these binders.

(2) In the case of PVP, most of the SiNPs in the anode are initially electrically connected by a continuous conductive network of carbon black, so that SiNPs not in direct contact with the current collector are still electrochemically active. Printed SiNP anodes prepared with PVP therefore exhibited high initial capacities. However, as the SiNPs expand and contract, they lose contact with the conductive carbon black, becoming electrically insulated and electrochemically inactive. The conductive network becomes disrupted after only a few lithiation and delithiation cycles and the battery's capacity rapidly decreases.

(3) In the case of PEDOT:PSS, there is initially a conductive network of carbon black, similar to the case with PVP. However, when SiNPs become disconnected from the carbon black network, they maintain electrical contact with the remainder of the electrode through the conductive PEDOT:PSS matrix. Printed SiNP anodes prepared with PEDOT:PSS thereby exhibited high initial capacities and more stable performance than anodes prepared with non-conductive polymer binders. This mechanism is also consistent with other reported conductive binders for Si electrodes, such as polypyrrole [62], polyaniline [41], and poly(9,9-dioctylfluorene-co-fluorenone-co-methylbenzoic acid) (PFFOMB) [63]. However, compared to other studies, the PEDOT:PSS solution used here is commercially available and no modification or polymerization is required.

Overall, the superior performance of the inkjet-printed silicon anodes with PEDOT:PSS binder can be attributed to the favourable properties of PEDOT:PSS. First, the PEDOT:PSS formulation used was specifically designed for use in inkjet printers, with optimal viscosity, surface tension, and density for ideal jetting conditions. It therefore
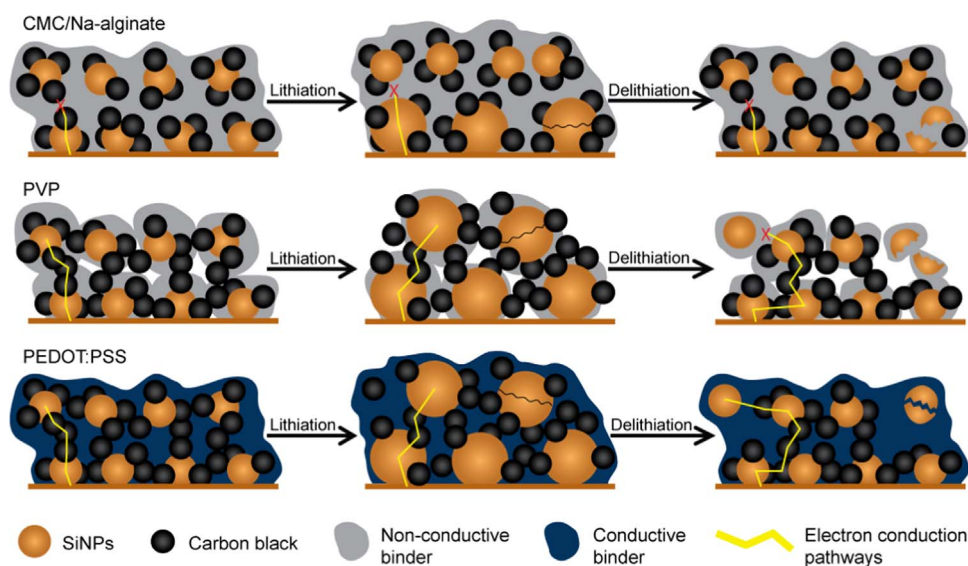
Fig. 4. Schematic illustration of the proposed mechanism explaining the electrochemical performance of anodes prepared with different binders. The use of non-conductive binders (CMC, Na-alginate, and PVP) leads to electrical isolation of SiNPs. In the case of CMC and Na-alginate, electrical isolation occurs from the start, leading to poor initial capacity, while in the case of PVP the conductive carbon black network is destroyed during large volume changes. With PEDOT:PSS, the SiNPs remain electrically connected throughout charging/discharging and are therefore able to maintain a stable cycling capacity.

readily formed uniform films without modification. Second, PEDOT:PSS is both electrically and ionically conductive. As shown by the SEM image, it is clear that the SiNP anodes printed with PEDOT:PSS binder are comprised of a single continuous matrix. A conductive network is maintained during cycling, ensuring that SiNPs do not become electrically isolated while simultaneously allowing lithium ions to migrate to and alloy with the SiNPs. This is one of the reasons for its superior cycling performance. Third, PEDOT:PSS is able to reversibly deform during cycling, allowing it to stretch and contract with the SiNPs and accommodate the large volume changes. It is also rigid enough to confine any particles that fracture during cycling. Additionally, there may be a chemical interaction between SiNPs and PEDOT:PSS that stabilizes the electrode structure during charging/discharging [43]. We believe that the understanding of the role of PEDOT:PSS binder in the inkjet-printed thin film SiNP electrodes revealed in this study can contribute to the future design and development of high performance anodes for thin film LIBs.

5. Conclusions

In conclusion, thin film SiNP anodes with various binders were fabricated by inkjet printing from the commercial available Si nano-particles for the first time. Inkjet printing resulted in very uniform, thin film electrodes with precise control over the thickness. The effect of the binder on cycling performance was investigated and anodes with PEDOT:PSS binder were the most stable, attributed to its electrical conductivity and reversible deformation upon electrode expansion and contraction. The continuous conductive network formed by PEDOT:PSS allows for rapid electron transfer and, at the same time, stretches to accommodate the large volume changes of SiNPs during charging and discharging. These anodes exhibit very high capacities of greater than 1700 mA h g^{-1} for 100 cycles, as well as very stable cycling performance when cycled at a limited depth-of-discharge of 1000 mA h g^{-1}, with over 1000 successful cycles. Anodes prepared with non-conductive polymer binders, on the other hand, had capacities that quickly degraded after only a few cycles. This was attributed to some SiNPs losing electrical contact with the remaining electrode each cycle, preventing them from contributing to capacity. This proposed mechanism was supported with SEM, FTIR, and Raman spectroscopy measurements. Overall, we have shown that inkjet printing is a viable fabrication method for high capacity thin film SiNP electrodes and that the polymer binder plays an important role in the electrochemical behaviour of printed electrodes. This technique may be extended to other electrode materials for the fabrication of a fully inkjet-printed cell when combined with an inkjet-printed electro-lyte.

Acknowledgements

Appendix A. Supporting information

Supplementary data associated with this article can be found in the online version at doi:10.1016/j.nanoen.2017.04.041.

References

[1] D. Wei, S. Haque, P. Andrew, J. Kivioja, T. Ryhänen, A. Pesquera, A. Centeno, B. Alonso, A. Chuvilin, A. Zurutuza, Ultrathin rechargeable all-solid-state batteries based on monolayer graphene, J. Mater. Chem. A 1 (2013) 3177–3781.

[2] S. Liu, Z. Wang, C. Yu, H.B. Wu, G. Wang, Q. Dong, J. Qiu, A. Eychmuller, X.W. David Lou, A flexible TiO(2)(B)-based battery electrode with superior power rate and ultralong cycle life, Adv. Mater. 25 (2013) 3462–3467.

[3] J. Schwenzel, V. Thangadurai, W. Weppner, Developments of high-voltage all-solid-state thin-film lithium ion batteries, J. Power Sources 154 (2006) 232–238.

[4] N. Li, Z. Chen, W. Ren, F. Li, H.-M. Cheng, Flexible graphene-based lithium ion batteries with ultrafast charge and discharge rates, Proc. Natl. Acad. Sci. USA 109 (2012) 17360–17365.

[5] N.J. Dudney, Thin film micro-batteries, Electrochem. Soc. Interface 17 (2008) 44–48.

[6] L. Hu, H. Wu, F. La Mantia, Y. Yang, Y. Cui, Thin, flexible secondary Li-ion paper batteries, ACS Nano 4 (2010) 5843–5848.

[7] P. Chen, H. Chen, J. Qiu, C. Zhou, Inkjet printing of single-walled carbon nanotube/RuO2 nanowire supercapacitors on cloth fabrics and flexible substrates, Nano Res. 3 (2010) 594–603.

[8] L.T. Le, M.H. Ervin, H. Qiu, B.E. Fuchs, W.Y. Lee, Graphene supercapacitor electrodes fabricated by inkjet printing and thermal reduction of graphene oxide, Electrochem. Commun. 13 (2011) 355–358.

[9] K.-H. Choi, J. Yoo, C.K. Lee, S.-Y. Lee, All-inkjet-printed, solid-state flexible supercapacitors on paper, Energy Environ. Sci. 9 (2016) 2812–2821.

[10] N. Stutzmann, R.H. Friend, H. Sirringhaus, Self-aligned, vertical-channel, polymer field- M. Ozkan, J. Eff. Transistors Sci. 299 (2003) 1881–1884.

[11] T. Kawase, T. Shimoda, C. Newsome, H. Sirringhaus, R.H. Friend, Inkjet printing of polymer thin film transistors, Thin Solid Films 438 (2003) 279–287.

[12] H. Azimi, Y. Hou, C.J. Brabec, Towards low-cost, environmentally friendly printed chalcopyrite and kesterite solar cells, Energy Environ. Sci. 7 (2014) 1829–1849.

[13] X. Lin, R. Klenk, L. Wang, T. Kohler, J. Albert, S. Fiechter, A. Ennaoui, M.C. Lux-Steiner, 11.3% efficiency Cu(In,Ga)(S,Se)2 thin film solar cells via drop-on-demand inkjet printing, Energy Environ. Sci. 9 (2016) 2037–2043.

[14] S.G. Hashmi, Halme, S.M. Zakeeruddin, J. Paltakari, M. Gratzel, P.D. Lund, Dye-sensitized solar cells with inkjet-printed dyes, Energy Environ. Sci. 9 (2016) 2453–2462.

[15] M.-S. Park, S.-H. Hyun, S.-C. Nam, Mechanical and electrical properties of a LiCoO2 cathode prepared by screen-printing for a lithium-ion micro-battery, Electrochim. Acta 52 (2007) 7895–7902.

[16] J. Huang, J. Yang, W. Li, W. Cai, Z. Jiang, Electrochemical properties of LiCoO2 thin film electrode prepared by ink-jet printing technique, Thin Solid Films 516 (2008) 3314–3319.

[17] C.A. Milroy, S. Jang, T. Fujimori, A. Dodabalapur, A. Manthiram, Inkjet-printed lithium–sulfur microcathodes for all-printed, integrated nanomanufacturing, Small (2017) 1603786.

[18] Y. Gu, A. Wu, H. Sohn, C. Nicoletti, Z. Iqbal, J.F. Federici, Fabrication of rechargeable lithium ion batteries using water-based inkjet printed cathodes, J. Manuf. Process. 20 (2015) 198–205.

[19] R.E. Sousa, C.M. Costa, S. Lanceros-Méndez, Advances and future challenges in printed batteries, ChemSusChem 8 (2015) 3539–3555.

[20] Y. Zhao, Q. Zhou, L. Liu, J. Xu, M. Yan, Z. Jiang, A novel and facile route of ink-jet printing to thin film SnO2 anode for rechargeable lithium ion batteries, Electrochim. Acta 51 (2006) 2639–2645.

[21] Y. Zhao, G. Liu, L. Liu, Z. Jiang, High-performance thin-film Li4Ti5O12 electrodes fabricated by using ink-jet printing technique and their electrochemical properties, J. Solid State Electrochem. 13 (2009) 705–711.

[22] H. Li, Z. Wang, L. Chen, X. Huang, Research on advanced materials for Li-ion batteries, Adv. Mater. 21 (2009) 4593–4607.

[23] M.T. McDowell, S.W. Lee, W.D. Nix, Y. Cui, 25th anniversary article: under-standing the lithiation of silicon and other alloying anodes for lithium-ion batteries, Adv. Mater. 25 (2013) 4966–4985.

[24] M.R. Zamfir, H.T. Nguyen, E. Moyen, Y.H. Lee, D. Pribat, Silicon nanowires for Li-based battery anodes: a review, J. Mater. Chem. A 1 (2013) 9566–9586.

[25] X. Su, Q. Wu, J. Li, X. Xiao, A. Lott, W. Lu, B.W. Sheldon, J. Wu, Silicon-based nanomaterials for lithium-ion batteries: a review, Adv. Energy Mater. 4 (2014) 1300882.

[26] B.A. Boukamp, G.C. Lesh, R.A. Huggins, All-solid lithium electrodes with mixed-conductor matrix, J. Electrochem. Soc. 128 (1981) 725–729.

[27] W.J. Weydanz, M. Wohlfahrt-Mehrens, R.A. Huggins, A room temperature study of the binary lithium–silicon and the ternary lithium–chromium–silicon system for use in rechargeable lithium batteries, J. Power Sources 81 (1999) 237–242.

[28] U. Kasavajjula, C. Wang, A.J. Appleby, Nano- and bulk-silicon-based insertion anodes for lithium-ion secondary cells, J. Power Sources 163 (2007) 1003–1039.

[29] X.H. Liu, L. Zhong, S. Huang, S.X. Mao, T. Zhu, J.Y. Huang, Size-dependent fracture of silicon nanoparticles during lithiation, ACS Nano 6 (2012) 1522–1531.

[30] H. Wu, Y. Cui, Designing nanostructured Si anodes for high energy lithium ion batteries, Nano Today 7 (2012) 414–429.

[31] C.K. Chan, H. Peng, G. Liu, K. McIlwrath, X.F. Zhang, R.A. Huggins, Y. Cui, High-performance lithium battery anodes using silicon nanowires, Nat. Nano 3 (2008) 31–35.

[32] M.-H. Park, M.G. Kim, J. Joo, K. Kim, J. Kim, S. Ahn, Y. Cui, J. Cho, Silicon nanotube battery anodes, Nano Lett. 9 (2009) 3844–3847.

[33] Y. Yao, M.T. McDowell, I. Ryu, H. Wu, N. Liu, L. Hu, W.D. Nix, Y. Cui, Interconnected silicon hollow nanospheres for lithium-ion battery anodes with long cycle life, Nano Lett. 11 (2011) 2949–2954.

[34] H. Kim, J. Cho, Superior lithium electroactive mesoporous Si@carbon core–shell nanowires for lithium battery anode material, Nano Lett. 8 (2008) 3688–3691.

[35] P. Gao, J. Fu, J. Yang, R. Lv, J. Wang, Y. Nuli, X. Tang, Microporous carbon coated silicon core/shell nanocomposite via in situpolymerization for advanced Li-ion

battery anode material, Phys. Chem. Chem. Phys. 11 (2009) 11101–11105.

[36] C. Wang, H. Wu, Z. Chen, M.T. McDowell, Y. Cui, Z. Bao, Self-healing chemistry enables the stable operation of silicon microparticle anodes for high-energy lithium-ion batteries, Nat. Chem. 5 (2013) 1042–1048.

[37] I. Kovalenko, B. Zdyrko, A. Magasinski, B. Hertzberg, Z. Milicev, R. Burtovyy, I. Luzinov, G. Yushin, A major constituent of brown algae for use in high-capacity Li-ion batteries, Science 334 (2011) 75–79.

[38] H. Buqa, M. Holzapfel, F. Krumeich, C. Veit, P. Novák, Study of styrene butadiene rubber and sodium methyl cellulose as binder for negative electrodes in lithium-ion batteries, J. Power Sources 161 (2006) 617–622.

[39] N.S. Hochgatterer, M.R. Schweiger, S. Koller, P.R. Raimann, T. Wöhrle, C. Wurm, M. Winter, Silicon/graphite composite electrodes for high-capacity anodes: influence of binder chemistry on cycling stability, Electrochem. Solid-State Lett. 11 (2008) A76.

[40] W.-R. Liu, M.-H. Yang, H.-C. Wu, S.M. Chiao, N.-L. Wu, Enhanced cycle life of Si anode for Li-ion batteries by using modified elastomeric binder, Electrochem. Solid-State Lett. 8 (2005) A100.

[41] H. Wu, G. Yu, L. Pan, N. Liu, M.T. McDowell, Z. Bao, Y. Cui, Stable Li-ion battery anodes by in-situ polymerization of conducting hydrogel to conformally coat silicon nanoparticles, Nat. Commun. 4 (2013) 1–6.

[42] S.D. Hoath, S. Jung, W.-K. Hsiao, I.M. Hutchings, How PEDOT:PSS solutions produce satellite-free inkjets, Org. Electron. 13 (2012) 3259–3262.

[43] D. Shao, H. Zhong, L. Zhang, Water-soluble conductive composite binder containing PEDOT:PSS as conduction promoting agent for Si anode of lithium-ion batteries, ChemElectroChem 1 (2014) 1679–1687.

[44] T.M. Higgins, S.-H. Park, P.J. King, C. Zhang, N. McEvoy, N.C. Berner, D. Daly, A. Shmeliov, U. Khan, G. Duesberg, V. Nicolosi, J.N. Coleman, A commercial conducting polymer as both binder and conductive additive for silicon nanoparticle-based lithium-ion battery negative electrodes, ACS Nano 10 (2016) 3702–3713.

[45] Y. Yang, G. Yu, J.J. Cha, H. Wu, M. Vosgueritchian, Y. Yao, Z. Bao, Y. Cui, Improving the performance of lithium–sulfur batteries by conductive polymer coating, ACS Nano 5 (2011) 9187–9193.

[46] F.M. Courtel, S. Niketic, D. Duguay, Y. Abu-Lebdeh, I.J. Davidson, Water-soluble binders for MCMB carbon anodes for lithium-ion batteries, J. Power Sources 196 (2011) 2128–2134.

[47] P.R. Das, L. Komsiyska, O. Osters, G. Wittstock, PEDOT:PSS as a functional binder for cathodes in lithium ion batteries, J. Electrochem. Soc. 162 (2015) A674–A678.

[48] N.J. Dudney, Y.-I. Jang, Analysis of thin-film lithium batteries with cathodes of 50 nm to 4 µm thick LiCoO2, J. Power Sources 119 (2003) 300–304.

[49] D. Lin, Z. Lu, P.-C. Hsu, H.R. Lee, N. Liu, J. Zhao, H. Wang, C. Liu, Y. Cui, A high tap density secondary silicon particle anode fabricated by scalable mechanical pressing for lithium-ion batteries, Energy Environ. Sci. 8 (2015) 2371–2376.

[50] C. Xu, F. Lindgren, B. Philippe, M. Gorgoi, F. Björefors, K. Edström, T. Gustafsson, Improved performance of the silicon anode for Li-ion batteries: understanding the surface modification mechanism of fluoroethylene carbonate as an effective electrolyte additive, Chem. Mater. 27 (2015) 2591–2599.

[51] Y.-M. Lin, K.C. Klavetter, P.R. Abel, N.C. Davy, J.L. Snider, A. Heller, C.B. Mullins, High performance silicon nanoparticle anode in fluoroethylene carbonate-based electrolyte for Li-ion batteries, Chem. Commun. 48 (2012) 7268–7270.

[52] C.-M. Park, J.-H. Kim, H. Kim, H.-J. Sohn, Li-alloy based anode materials for Li secondary batteries, Chem. Soc. Rev. 39 (2010) 3115–3141.

[53] S. Komaba, N. Yabuuchi, T. Ozeki, Z.-J. Han, K. Shimomura, H. Yui, Y. Katayama, T. Miura, Comparative study of sodium polyacrylate and poly(vinylidene fluoride) as binders for high capacity Si–graphite composite negative electrodes in Li-ion batteries, J. Phys. Chem. C 116 (2011) 1380–1389.

[54] C. Sriprachuabwong, C. Karuwan, A. Wisitsorrat, D. Phokharatkul, T. Lomas, P. Sritongkham, A. Tuantranont, Inkjet-printed graphene-PEDOT:PSS modified screen printed carbon electrode for biochemical sensing, J. Mater. Chem. 22 (2012) 5478–5485.

[55] Y. Xiao, J.-Y. Lin, S.-Y. Tai, S.-W. Chou, G. Yue, J. Wu, Pulse electropolymerization of high performance PEDOT/MWCNT counter electrodes for Pt-free dye-sensitized solar cells, J. Mater. Chem. 22 (2012) 19919–19925.

[56] D. Pavia, G. Lampman, G. Kriz, J. Vyvyan, Introduction to Spectroscopy, Cengage Learning, Belmont, CA, 2009.

[57] M. Marti, G. Fabregat, F. Estrany, C. Aleman, E. Armelin, Nanostructured conducting polymer for dopamine detection, J. Mater. Chem. 20 (2010) 10652–10660.

[58] A. Xiao, L. Yang, B.L. Lucht, S.-H. Kang, D.P. Abraham, Examining the solid electrolyte interphase on binder-free graphite electrodes, J. Electrochem. Soc. 156 (2009) A318–A327.

[59] M. Nie, D.P. Abraham, Y. Chen, A. Bose, B.L. Lucht, Silicon solid electrolyte interphase (SEI) of lithium ion battery characterized by microscopy and spectroscopy, J. Phys. Chem. C 117 (2013) 13403–13412.

[60] T. Zhang, H. Zhou, A reversible long-life lithium–air battery in ambient air, Nat. Commun. 4 (2013) 1–7.

[61] Y. Yao, N. Liu, M.T. McDowell, M. Pasta, Y. Cui, Improving the cycling stability of silicon nanowire anodes with conducting polymer coatings, Energy Environ. Sci. 5 (2012) 7927–7930.

[62] Z. Du, S. Zhang, Y. Liu, J. Zhao, R. Lin, T. Jiang, Facile fabrication of reticular polypyrrole-silicon core-shell nanofibers for high performance lithium storage, J. Mater. Chem. 22 (2012) 11636–11641.

[63] G. Liu, S. Xun, N. Vukmirovic, X. Song, P. Olalde-Velasco, H. Zheng, V.S. Battaglia, L. Wang, W. Yang, Polymers with tailored electronic structure for high capacity lithium battery electrodes, Adv. Mater. 23 (2011) 4679–4683.

Stephen Lawes received his Bachelor of Applied Science in Nanotechnology Engineering from the University of Waterloo, Canada in 2013. He then completed a Masters in Mechanical and Materials Engineering from Western University, Canada in 2015 under the supervision of Prof. Xueliang (Andy) Sun, during which his research focused on inkjet printing of thin film batteries. He joined OXIS Energy, UK, as a research scientist in 2015, where he is currently working on lithium protection for lithium-sulfur batteries.

Dr. Qian Sun is a postdoctoral fellow in Prof. Xueliang (Andy) Sun's Group at the University of Western Ontario, Canada. He received his B.S. degree in Chemistry in 2006, M.S. degree in Physical Chemistry in 2009, and Ph.D. degree in Applied Chemistry in 2013 at Fudan University, China, under the supervision of Prof. Dr. Zheng-Wen Fu on the study of Li-/Na-ion batteries and Na-air batteries. He joined Prof. Sun's group in 2013 and his current research interests focus on Na-air, Na-S, and Na-ion batteries as well as solid-state Li/Na batteries.

Andrew Lushington received his B.Sc in Chemistry with a Concentration in Nanotechnology from Carleton University, Ottawa, Canada in 2012. He is currently pursuing a Ph.D. in the department of Mechanical and Materials Engineering at Western University in London, Ontario, Canada and started in 2013. His research interests include Atomic Layer Deposition and Molecular Layer Deposition for energy storage and energy conversion application. His research also includes the use of synchrotron radiation to study thin-film and catalyst properties.

Dr. Biwei Xiao graduated from Prof. Xueliang (Andy) Sun's group at the University of Western Ontario as a Ph.D. He is currently a postdoctoral research associate at the Pacific Northwest National Laboratory. His research interests are associated with the synthesis, modification and mechanism study of electrode materials for lithium-ion batteries and sodium-ion batteries, atomic layer deposition, synchrotron radiation technique and carbonaceous materials.

Yulong Liu is currently a Ph.D. candidate in Prof. Xueliang (Andy) Sun' Nanomaterials and Energy Group at the University of Western Ontario, Canada. He received his Bachelor degree from Central South University, China, in 2010, and Master degree in 2013. His research interests include nanomaterials for lithium ion batteries, especially LiFePO4 (in collaboration with *Phostech Lithium Inc.*), and the development of the solid state batteries.

Prof. Xueliang (Andy) Sun is a Canada Research Chair in Development of Nanomaterials for Clean Energy, Fellow of the Royal Society of Canada and Canadian Academy of Engineering and Full Professor at the University of Western Ontario, Canada. Dr. Sun received his Ph.D. in materials chemistry in 1999 from the University of Manchester, UK, which he followed up by working as a postdoctoral fellow at the University of British Columbia, Canada and as a Research Associate at L'Institut National de la Recherche Scientifique (INRS), Canada. His current research interests are focused on advanced materials for electrochemical energy storage and conversion, including electrocatalysis in fuel cells and electrodes in lithium-ion batteries and metal–air batteries.